ROYAL SOCIETY OF CHEMISTRY

PAPER

Check for updates

Formation of an NIR-emitting Ag$_{34}$S$_3$SBB$_{20}$(CF$_3$COO)$_6$$^{2+}$ cluster from a hydride-protected silver cluster†

C. K. Manju, [ID] Debasmita Ghosh, Mohammad Bodiuzzaman [ID] and Thalappil Pradeep [ID] *

Recent reports have shown that the intercluster reaction is a new synthetic strategy to prepare alloy clusters. In this work, we performed an intercluster reaction between silver clusters and produced highly ionizable Ag–S-type clusters; we examined their formation by mass spectrometry. [Ag$_{18}$(TPP)$_{10}$H$_{16}$]$^{2+}$ (Ag$_{18}$), a highly reactive hydride and phosphine-protected silver cluster, was used as a sacrificial cluster in this synthesis. An intercluster reaction between Ag$_{18}$ and smaller silver-chalcogenolate clusters (SCC) resulted in a new cluster, [Ag$_{34}$S$_3$SBB$_{20}$(CF$_3$COO)$_6$]$^{2+}$. The cluster showed an NIR emission at around 1100 nm. The cluster composition was confirmed by high-resolution electrospray ionization mass spectrometry (ESI-MS), thermogravimetry (TGA), and X-ray photoelectron spectroscopy (XPS).

Introduction

Nanoclusters (NCs) of noble metals and semiconductors have been of significant interest in contemporary science due to their chemical and physical properties and a wide variety of applications.[1–3] NCs consisting of a few atoms have properties that are in between those of molecules and bulk materials. These NCs show size-dependent optical characteristics.[3,4] Different synthetic methodologies have been reported to prepare these NCs.[1,5] Various spectroscopic and spectrometric techniques have been employed to understand them in detail, including UV-visible spectroscopy (UV-vis), photo-luminescence, nuclear magnetic resonance (NMR), matrix-assisted laser desorption ionization mass spectrometry (MALDI MS), electrospray ionization mass spectrometry (ESI-MS), and single crystal X-ray diffraction (XRD).[2,5–10]

Several chalcogenide clusters of silver, copper, cadmium, and zinc (Ag, Cu, Cd, and Zn) have been investigated.[11–15] Historically, a coordination chemistry approach has been followed for the synthesis of high-nuclearity metal chalcogenide clusters.[11] In this approach, the reaction of a metal salt (MX)

DST Unit of Nanoscience (DST UNS) and Thematic Unit of Excellence,
Department of Chemistry, Indian Institute of Technology Madras, Chennai 600036,
India. E-mail: pradeep@iitm.ac.in

†Electronic supplementary information (ESI) available: UV-vis and ESI-MS spectra of Ag$_{18}$, ESI-MS spectrum of 30 min reaction product, comparative IR spectra of cluster and CF$_3$COOAg, XPS spectrum of cluster, SEM EDS spectrum and mapping, and UV-vis and ESI spectra of control experiments. See DOI: 10.1039/c9dt01533g

with a chalcogenide precursor or highly reactive thiolates and phosphines resulted in chalcogenide clusters. Silylated compounds such as E(SiMe$_3$)$_2$ and RESiMe$_3$ (E = S, Se, Te) along with mono or diphosphines were used. The highly polarizable electrons and the anionic nature of these ligands helped the formation of clusters with different bridging modes. The choice of MX and the presence of phosphines were the critical factors in this method. A large number of crystal structures were reported using this method including that of the largest Ag$_{490}$S$_{118}$(S^{t}C$_5$H$_{11}$)$_{114}$.[14,16,17] The inherent insoluble nature of these clusters made their solution phase studies difficult. This issue was recently resolved by the use of 4-tert-butylbenzyl mercaptan as a capping agent.[18]

The insertion reaction of CS$_2$ into the M–S bond is another way to synthesize chalcogenide clusters.[19] Larger Cd–S clusters can be obtained by the reaction of cadmium thiolates with CS$_2$.[20] The slow release of S^{2-} is due to the reaction of CS$_2$ with solvents. S^{2-} can be released into the reaction medium by the cleavage of the C–S bond, which results in the Ag–S cluster core.[21,22] Clusters such as Ag$_{62}$S$_{13}$(S^{t}Bu)$_{32}$$^{4+}$ and Ag$_{62}$S$_{12}$(S^{t}Bu)$_{32}$$^{2+}$ are formed by the cleavage of t-Butyl mercaptan (^{t}BuSH). A change in the number of core sulfur atoms has a large impact on the physical properties of these clusters. Ag$_{62}$S$_{13}$(S^{t}Bu)$_{32}$$^{4+}$ was highly red luminescent both in solution and in the solid state, while the luminescence was quenched in Ag$_{62}$S$_{12}$(S^{t}Bu)$_{32}$$^{2+}$. Femtosecond transient absorption spectra suggested that the quenching of luminescence in the latter cluster was due to the free valence electrons available.[22]

Synthetic methods for noble metal clusters include the Brust–Schiffrin method and its modifications,[23,24] ligand-

induced etching of NPs,[25] ligand exchange (thiolates with sele-nolates),[26] solid state,[27] and ligand exchange-induced size transformation (LEIST).[28,29] Recent reports have shown the intercluster reaction as a new pathway to produce alloy clusters.[30,31] Here, thiolate-protected clusters of two different metals were allowed to react. The reaction resulted in the exchange of metal ions and ligands. This methodology can also be extended to the clusters of same metals.

Fluorescence is one of the important properties of NCs, due to which they find applications in the field of chemical sensing, bioimaging, and drug delivery.[32] Most of the reported clusters emit in the red region.[33] There have been many efforts to tune the luminescence of NCs by changing the ligand composition and core size or by heteroatom doping. Near-infrared (NIR)-emitting materials find more applications in the field of biomedical science and energy conversion. Compared with optical imaging in the visible (450–700 nm) and NIR-I (700–950 nm) regions, the NIR-II (1000–1400 nm) region is optimal because of the lower auto-fluorescence and reduced scattering.[32] Silver chalcogenide semiconductors of a lower band gap, which emit in the NIR-II window, have been used for bio-imaging applications.[32]

In this work, we describe the synthesis of a new Ag–S cluster from a highly reactive silver cluster protected by phosphine and hydrides. The new cluster was assigned as $[Ag_{34}S_3SBB_{20}(CF_3COO)_6]^{2+}$ from the ESI-MS, TGA, and EDS data. An intercluster reaction of two silver clusters produced a cluster of different nuclearity. This protocol resulted in a charged cluster, which made the ESI-MS studies possible compared to our earlier efforts to make easily ionizable chalcogenide clusters. The cluster showed emission in solution and in the solid state at around 1100 nm.

Materials and methods

Materials

Silver nitrate (AgNO₃), silver trifluoroacetate (CF₃COOAg), 4-*tert*-butylbenzyl mercaptan (BBSH), triphenyl phosphine (TPP) and sodium borohydride (NaBH₄) were purchased from Sigma Aldrich, India. Methanol (MeOH), chloroform, aceto-nitrile (ACN), hexane and dichloromethane (DCM) were obtained from Merck India.

Synthesis of thiolate (Ag-SBB)

Silver thiolate was prepared by using a 1 : 5 mmol ratio of AgNO₃ and BBSH. About 169 mg of AgNO₃ was dissolved in 7 mL of MeOH by sonication for 5 minutes. Then, 933 µl of BBSH was added drop by drop. The reaction mixture was stirred for 1 h. After that, the light yellowish product was cen-trifuged and washed with MeOH four times and dried using a rotavapor.

Synthesis of $[Ag_{18}(TPP)_{10}H_{16}]^{2+}$

$[Ag_{18}(TPP)_{10}H_{16}]^{2+}$ was synthesized by following a previously reported method.[34] In a typical synthesis, 20 mg of AgNO₃ (or 25 mg CF₃COOAg) was dissolved in 1.5 mL of MeOH by soni-cation. This was added to a vial containing 3.5 mL of MeOH. Then, 70 mg of PPh₃ dissolved in 10 mL of chloroform was added to the mixture under stirring conditions. After 20 minutes of stirring, 6.5 mg of NaBH₄ dissolved in 0.5 mL cold water was added. The solution turned yellow immediately after the addition of NaBH₄ solution. Green-colored Ag₁₈ was obtained after 3 h of stirring. This green solution was dried and washed with water. After a water wash, the green precipi-tate was dried and dissolved in the required amount of MeOH and used for further synthesis.[34]

Synthesis of $Ag_{34}S_3SBB_{20}(CF_3COO)_6{}^{2+}$

About 0.35 mmol of Ag-SBB was suspended in 3 mL of ACN. ACN (1 mL) containing 0.45 mmol of CF₃COOAg was added to the above solution under continuous stirring. After 3 min of stirring, 2 mL of Ag₁₈ (absorbance at 545 nm was kept as 0.9) was added to this mixture. The color of the solution changed from yellow to brown. Stirring was continued for 4.5 h, and the obtained suspension was centrifuged and washed with MeOH. The resulting precipitate was dissolved in hexane and centri-fuged. A brown-colored supernatant was collected, and the pre-cipitate was discarded. The purified cluster was soluble in DCM, hexane, toluene, and heptane.

Instrumentation

Absorbance spectra were measured using a PerkinElmer Lambda 365 instrument in the range of 200–1100 nm. A Waters Synapt G2Si HDMS instrument consisting of an electro-spray source, quadrupole ion guide/trap, ion mobility cell, and TOF analyzer was used for the ESI-MS measurements. CID measurements were obtained by colliding with high-purity Ar gas. All the ESI-MS spectra were measured in the positive mode. The ESI-MS sample was prepared by dissolving 1 mg of the cluster in 1 mL DCM. Then, 200 µl of this was diluted to 2 mL and used for the electrospray measurements. Thermogravimetric (TG) analyses were carried out on a PerkinElmer TGA7 instrument under N₂ atmosphere. A FEI quanta 200 scanning electron microscope fitted with a tung-sten filament was used for the energy dispersive spectroscopy (EDS) measurements. X-ray photoelectron spectroscopy (XPS) was conducted using an Omicron ESCA probe spectrometer with polychromatic Mg Kα X-rays ($h\nu$ = 1253.6 eV). IR measure-ments were obtained using a PerkinElmer Spectrum Two instrument. A Jobin Yvon NanoLog instrument was used for the photoluminescence measurements.

Results and discussion

The recently reported hydride-protected $[Ag_{18}(TPP)_{10}H_{16}]^{2+}$ (abbreviated as Ag₁₈ hereafter) was used as a sacrificial cluster for the synthesis of a new Ag–S cluster.[34] Ag₁₈ was synthesized by a modified procedure previously reported by our group.[35] The purified Ag₁₈ was dissolved in MeOH and characterized by UV-vis and ESI-MS (Fig. S1†). Ag₁₈ showed two main UV-vis

absorption peaks at 545 nm and 614 nm. A peak at m/z 2290 in the positive ion mode ESI-MS confirmed the formation of Ag_{18}.

In a typical synthesis, an MeOH solution of the Ag_{18} cluster was added to a mixture of Ag-SBB and CF_3COOAg in ACN. The addition of Ag_{18} to this mixture resulted in a color change from yellow to brown. The reaction was continued until the supernatant of the mixture became clear. A hexane solution of the new cluster showed two main peaks at 497 and 618 nm and two humps at 457 and 690 nm (Fig. 1A) in the UV-vis measurement. These features were different from those of Ag_{18} used as the reagent and other reported clusters.[36–39] The cluster showed an emission around 1100 nm when excited at 497 nm both in solution and in the solid state (inset of Fig. 1A). An ESI-MS measurement of the cluster dissolved in DCM showed an intense peak at 3676 m/z in the positive mode (Fig. 1B). This peak is expanded in the inset of Fig. 1B, which shows a peak separation of 0.5 mass unit, confirming the 2+ charge state of the cluster ion. The composition of $Ag_{34}S_3SBB_{20}{}^{2+}$ was assigned to this cluster from the isotopic distribution pattern, which is in good agreement with the observation of the theoretical spectrum (blue) shown in the inset of Fig. 1B.

A time-dependent experiment was also performed to monitor the synthesis process. The UV-vis spectrum of the time-dependent reaction showed a small peak shift from 30 min to 1 h of the reaction. After 1 h, there was no change in the UV-vis spectrum (Fig. 2A). The ESI-MS measurements of the time-dependent cluster synthesis showed an envelope of peaks with a 2+ charge state around m/z 5000 after 30 minutes of reaction (Fig. 2B). From 1 h onwards, the species at m/z 3676 became the intense one. This suggested that larger clusters were formed in the initial stages of the reaction and they decomposed to a stable smaller cluster. The higher intensity peak for the 30 min sample could be assigned to a compo-

sition of $Ag_{47}S_7SBB_{28}{}^{2+}$ (m/z 5156) (Fig. S2†). Two other peaks at m/z 5013 and 4869 were assigned to the loss of the Ag-SBB group from the main peak. The lower mass range ESI-MS spectra showed peaks corresponding to thiolates with the general formula $Ag_nSBB_mS_xCF_3COO_y$ (Fig. S3, Table S1†).

Tandem mass spectrometric (MS/MS) studies were performed to understand the cluster in more detail (Fig. 3A). The collision-induced dissociation (CID) of well-known silver nanoclusters showed that their solution phase stability is reflected in the gas phase dissociation.[40] The peak at m/z 3676 was selected for CID experiments. Measurements were obtained by gradually increasing the collision energy (CE, in instrumental units) of the selected ions and after colliding with Ar. The first fragmentation started at CE 25. Two peaks were observed under this condition, which were assigned to the loss of Ag_3SBB_3 and Ag_4SBB_4 from the main cluster. The peak corresponding to the loss of Ag_4SBB_4, giving rise to $Ag_{30}S_3(SBB)_{16}{}^{2+}$, was the dominant one. This observation was similar to the fragmentation of $Ag_{25}(SR)_{18}{}^-$, where the loss of neutral Ag_4SR_4 gives $Ag_{21}(SR)_{14}{}^-$ as the prominent species.[41] A fragmentation study of $Ag_{25}(SR)_{18}{}^-$ showed that upon increasing CE, the Ag_3SR_3 unit was lost from $Ag_{25}(SR)_{18}{}^-$.[40] In the present study, a further increase in the collision energy resulted in Ag_6SBB_6 and Ag_7SBB_7 losses from $Ag_{34}S_3SBB_{20}{}^{2+}$. The parent ion intensity started decreasing from CE 40 and at CE 50, the intensity of the peak $Ag_{27}S_3SBB_{13}{}^{2+}$, arising from the loss of Ag_7SBB_7 became the prominent one. Ten Ag-SBB losses were observed in the MS/MS measurements. In the lower mass range, fragments such as $Ag_5SBB_4{}^+$, $Ag_6SBB_5{}^+$, $Ag_7SBB_6{}^+$ and $Ag_8SBB_7{}^+$ were also observed as the CE increased (Fig. S4).† $Ag_6SBB_5{}^+$ was the dominant species in this region.

A careful analysis of the higher m/z region of the ESI-MS spectra showed less intense peaks, which could be assigned to the attachment of the trifluoroacetate (CF_3COO^-) groups to the $Ag_{34}S_3SBB_{20}{}^{2+}$ cluster (Fig. 3B). A maximum of six CF_3COO^-
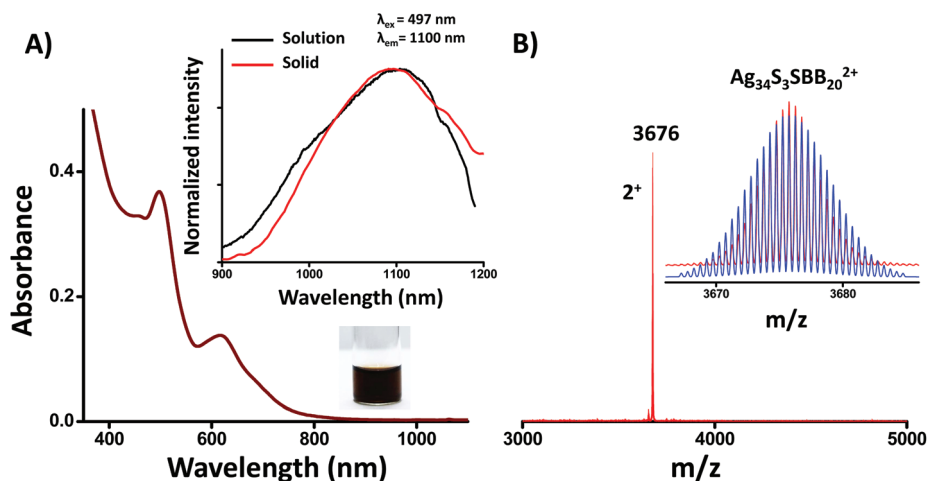

Fig. 1 (A) UV-vis spectrum of the purified cluster in hexane showing absorption features at 457, 497, 618, and 690 nm. The luminescence spectrum of the cluster in the solution and solid state showing emission maxima around 1100 nm is given in the inset. A photograph of the cluster solution is also shown in the inset. (B) Positive mode ESI-MS spectrum of the cluster. The peak at m/z 3676 is expanded and compared with the theoretical isotopic pattern (red–experimental and blue–theoretical), which matches with the composition of $Ag_{34}S_3SBB_{20}{}^{2+}$.
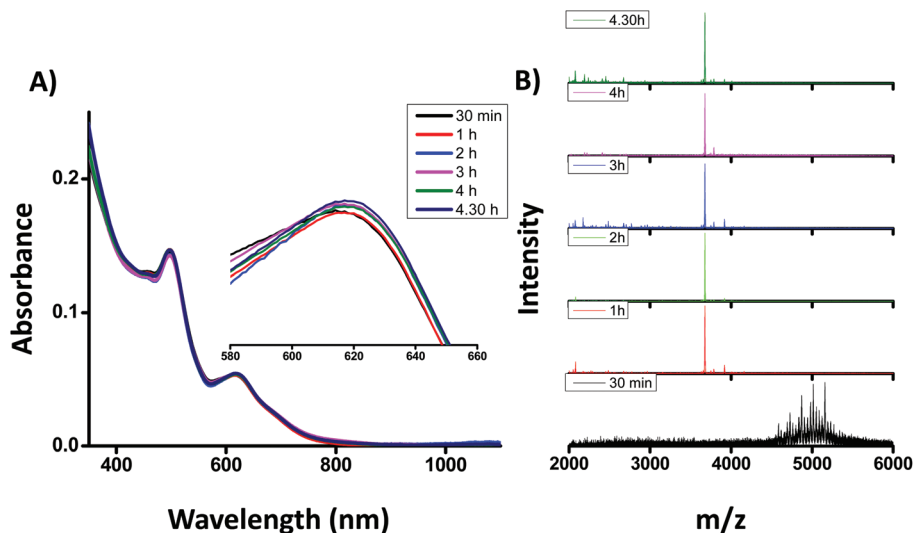
Fig. 2 (A) Time-dependent UV-vis absorption and (B) ESI-MS spectra of the cluster. The reaction was continued till 4.5 h. The absorption feature at the 618 nm region is expanded in the inset of (A), showing a small peak shift from 30 minutes to 1 h. Correspondingly, ESI-MS also showed certain changes (B).
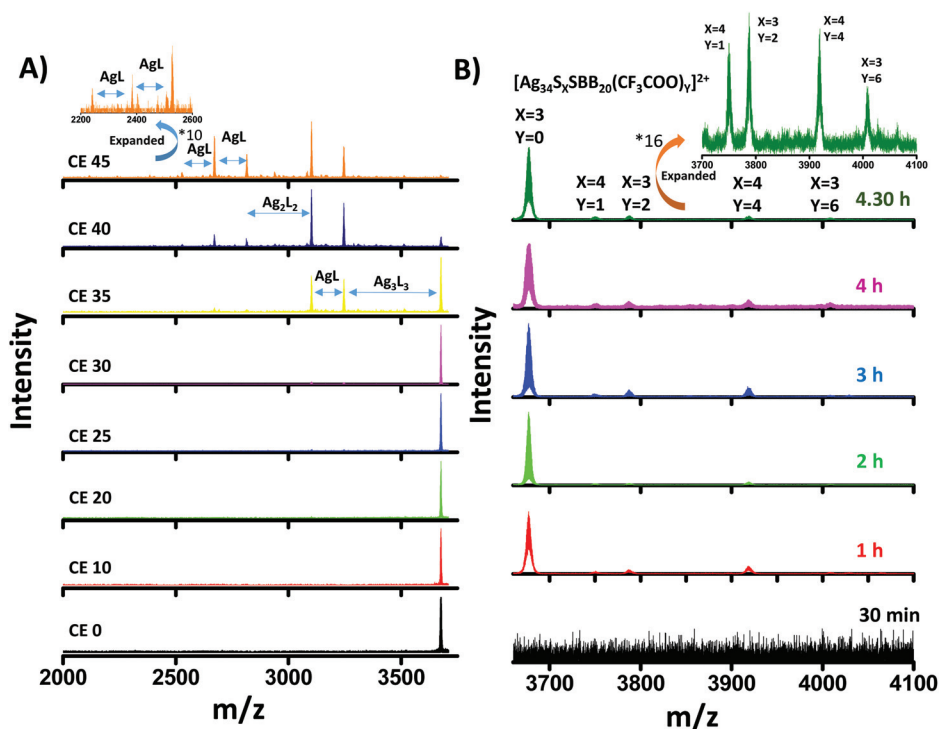

Fig. 3 Collision energy (CE)-dependent ESI-MS spectra of the m/z 3676 peak (A). We have marked CE (in instrumental units). Loss of neutral Ag_nSBB_n units was observed during the measurement. Time-dependent ESI-MS spectra expanded in the higher m/z region are given in (B). Peaks corresponding to the CF_3COO^- group attachment to the main peak (m/z 3676) were seen with low intensity in this region. $Ag_{34}S_4SBB_{20}^{2+}$ formed as a by-product is also observed with the CF_3COO^- attachment.

attachments were observed. A small amount of $Ag_{34}S_4SBB_{20}^{2+}$ formed as a byproduct was also seen with the CF_3COO^- attachment. This secondary ligand may be labile in nature and hence, it was less intense in the mass spectrum. We did not observe any change in the charge state after ligand desorption.

The charge of the cluster may be due to the cluster core arising from the magic number of electrons needed for electronic stability. It is likely that the ligand loss is not affecting the overall charge of the cluster as the ligands may be leaving as neutral entities. Carboxylates can undergo decarboxylation

and neutral species can be formed.[42] The decarboxylation of Ag-LA (LA = Lipoic acid) was observed during the ESI MS studies.[43] The fragmentation of thiolates as RH and RS-SR was also seen without a change in the charge state.[44] The four peaks observed in this region were assigned to $[Ag_{34}S_4SBB_{20}(CF_3COO)]^{2+}$, $[Ag_{34}S_3SBB_{20}(CF_3COO)_2]^{2+}$, $[Ag_{34}S_4SBB_{20}(CF_3COO)_4]^{2+}$, and $[Ag_{34}S_3SBB_{20}(CF_3COO)_6]^{2+}$. The intensity of the six CF_3COO^- attached peaks increased with time.

Infrared spectroscopic (IR) measurements were obtained to confirm the presence of CF_3COO^- as the secondary ligand. Comparative IR spectra of the cluster and the BBSH ligand and the cluster and CF_3COOAg are given in Fig. 4 and Fig. S5,† respectively. The IR spectrum of the cluster showed some new peaks along with BBSH features (Fig. 4A). New features at 720, 1137, and 1197 cm^{-1} were assigned to the CF_3 group. A strong peak at 1648 cm^{-1} was due to the carbonyl (C=O) stretching. The carbonyl stretching of the cluster showed a small shift towards a higher wavenumber in comparison to the observation for pure CF_3COOAg. The important difference between a thiol-protected cluster and a pure thiol is the disappearance of the S–H vibration at around 2562 cm^{-1} (Fig. 4B). This confirmed the formation of the metal-sulfur bond. The aliphatic C–H stretching region is around 2850–2950 cm^{-1} and the aromatic C–H stretching peaks appear at around 3000–3100 cm^{-1}. After cluster formation, the aromatic C–H stretching was not prominent. An earlier study of thiol-protected gold clusters showed the overlap of aromatic and aliphatic C–H stretchings.[45]

XPS measurements confirmed the presence of silver, sulfur, and fluorine in the synthesized cluster. Silver showed a higher binding energy compared to Ag(0) (368.0 eV), which confirmed the presence of Ag in the univalent state (Fig. S6†). Thermogravimetric (TG) analysis of the cluster showed 54.3% weight loss due to organic ligands (Fig. 5). A cluster composition of $[Ag_{34}S_3SBB_{20}(CF_3COO)_6]^{2+}$ with two CF_3COO^- groups as the counter ions matched this mass loss. The SEM EDS
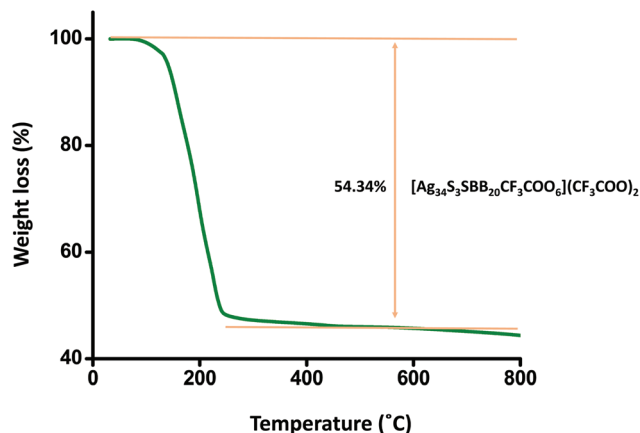
Fig. 5 TG curve of the cluster showing 54.3% weight loss. The loss corresponded to the composition of $[Ag_{34}S_3SBB_{20}CF_3COO_6](CF_3COO)_2$.

result with an Ag : S : F ratio of 1 : 0.64 : 0.71 was also in good agreement with the assigned formula (Fig. S7†).

To understand the factors affecting cluster formation, different control experiments were performed. The first one involved the determination of the role of CF_3COOAg in synthesis. In this case, Ag_{18} was added to a suspension of Ag-SBB in ACN. The reaction was continued for 4.5 h. After that, the product was purified by hexane precipitation. The product formed was red in color and showed an absorption at 440 nm, which was different from that of the CF_3COOAg-added cluster (Fig. S8†). Similarly, we tried an experiment with Ag_{18} synthesized using CF_3COOAg as the precursor, which may have CF_3COO^- groups as counter ions. In this case, the product formed was also different and showed a broad absorption at 465 nm (Fig. S9†). From these control experiments, it was understood that the addition of CF_3COOAg was crucial in this synthesis. In order to understand the role of CF_3COOAg in the synthesis, the yellow solution formed after the addition CF_3COOAg to Ag-SBB was further investigated. The UV-vis
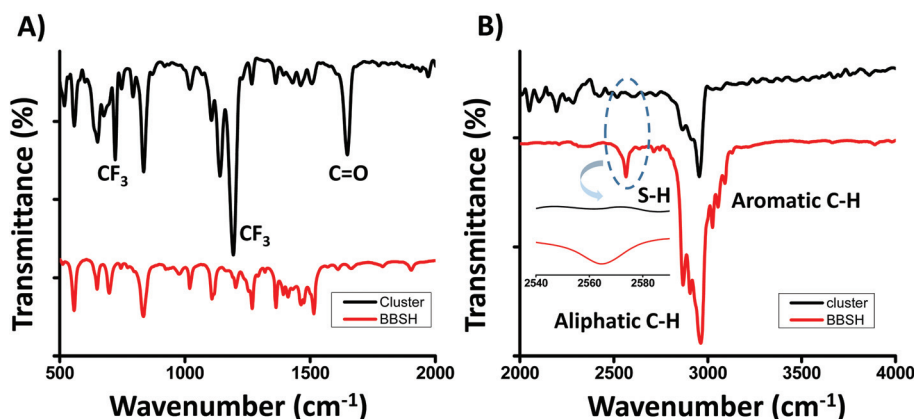
Fig. 4 Comparison of the IR spectra of the cluster and pure BBSH thiol. The cluster showed IR features of both thiol and CF_3COO^- groups (A and B). The IR features of the CF_3COO^- group were seen at 720, 1137 and 1197 cm^{-1} (due to CF_3) as well as at 1648 cm^{-1} (due to C=O). The formation of the metal−sulfur bond is clear from the absence of the S−H vibration at 2562 cm^{-1} for the cluster; this region is expanded in the inset.

spectrum of this solution showed two humps at 235 and 290 nm (Fig. S10†). To obtain more details, ESI-MS of this solution was also measured. The ESI-MS studies (Fig. S11†) showed that smaller silver-chalcogenolate clusters (SCC) were formed in the solution by the reaction of thiolate and CF_3COOAg. The formation of SCC by the reaction of Ag-thiolates with CF_3COOAg is known in the case of SCC metal–organic frameworks (MOFs).[46] These SCCs formed were reacted with Ag_{18}, and new clusters were obtained.

Conclusions

In conclusion, we synthesized a new Ag–S-type cluster and characterized it using various techniques including ESI-MS, UV-vis, TGA, IR, and XPS. A reaction between a hydride and phosphine-protected silver cluster and silver-chalcogenolate clusters produced the new cluster. The UV-vis spectrum showed four absorption features at 497, 457, 618, and 690 nm. The cluster showed NIR-II (1000–1400 nm) emission around the 1100 nm region, which is the ideal window for bio-imaging. The prominent ESI-MS peak at m/z 3676 was assigned to the composition of $Ag_{34}S_3SBB_{20}{}^{2+}$. A detailed investigation using ESI-MS and other techniques such as TGA and EDS pointed to a composition of $[Ag_{34}S_3SBB_{20}(CF_3COO)_6]^{2+}$ for the cluster with CF_3COO^- as counter ions.

Conflicts of interest

There are no conflicts to declare.

Acknowledgements

References

1 A. Mathew and T. Pradeep, *Part. Part. Syst. Charact.*, 2014, **31**, 1017–1053.

2 R. Jin, C. Zeng, M. Zhou and Y. Chen, *Chem. Rev.*, 2016, **116**, 10346–10413.

3 J. F. Corrigan, O. Fuhr and D. Fenske, *Adv. Mater.*, 2009, **21**, 1867–1871.

4 V. N. Soloviev, A. Eichhoefer, D. Fenske and U. Banin, *J. Am. Chem. Soc.*, 2001, **123**, 2354–2364.

5 Y.-P. Xie, J.-L. Jin, G.-X. Duan, X. Lu and T. C. W. Mak, *Coord. Chem. Rev.*, 2017, **331**, 54–72.

6 A. Dass, A. Stevenson, G. R. Dubay, J. B. Tracy and R. W. Murray, *J. Am. Chem. Soc.*, 2008, **130**, 5940–5946.

7 A. Desireddy, B. E. Conn, J. Guo, B. Yoon, R. N. Barnett, B. M. Monahan, K. Kirschbaum, W. P. Griffith, R. L. Whetten, U. Landman and T. P. Bigioni, *Nature*, 2013, **501**, 399–402.

8 H. Yang, Y. Wang, H. Huang, L. Gell, L. Lehtovaara, S. Malola, H. Hakkinen and N. Zheng, *Nat. Commun.*, 2013, **4**, 2422.

9 M. Zhu, C. M. Aikens, F. J. Hollander, G. C. Schatz and R. Jin, *J. Am. Chem. Soc.*, 2008, **130**, 5883–5885.

10 P. D. Jadzinsky, G. Calero, C. J. Ackerson, D. A. Bushnell and R. D. Kornberg, *Science*, 2007, **318**, 430–433.

11 O. Fuhr, S. Dehnen and D. Fenske, *Chem. Soc. Rev.*, 2013, **42**, 1871–1906.

12 N. Herron, J. C. Calabrese, W. E. Farneth and Y. Wang, *Science*, 1993, **259**, 1426–1428.

13 I. G. Dance, A. Choy and M. L. Scudder, *J. Am. Chem. Soc.*, 1984, **106**, 6285–6295.

14 C. Anson, A. Eichhoefer, I. Issac, D. Fenske, O. Fuhr, P. Sevillano, C. Persau, D. Stalke and J. Zhang, *Angew. Chem., Int. Ed.*, 2008, **47**, 1326–1331.

15 Y. Wang, Y.-H. Liu, Y. Zhang, F. Wang, P. J. Kowalski, H. W. Rohrs, R. A. Loomis, M. L. Gross and W. E. Buhro, *Angew. Chem., Int. Ed.*, 2012, **51**, 6154–6157.

16 D. Fenske, C. E. Anson, A. Eichhoefer, O. Fuhr, A. Ingendoh, C. Persau and C. Richert, *Angew. Chem., Int. Ed.*, 2005, **44**, 5242–5246.

17 R. Langer, B. Breitung, L. Wuensche, D. Fenske and O. Fuhr, *Z. Anorg. Allg. Chem.*, 2011, **637**, 995–1006.

18 S. Bestgen, O. Fuhr, B. Breitung, V. S. Kiran Chakravadhanula, G. Guthausen, F. Hennrich, W. Yu, M. M. Kappes, P. W. Roesky and D. Fenske, *Chem. Sci.*, 2017, **8**, 2235–2240.

19 K. Tang, X. Xie, Y. Zhang, X. Zhao and X. Jin, *Chem. Commun.*, 2002, 1024–1025, DOI: 10.1039/b201116f..

20 X. Jin, K. Tang, S. Jia and Y. Tang, *Polyhedron*, 1996, **15**, 2617–2622.

21 G. Li, Z. Lei and Q.-M. Wang, *J. Am. Chem. Soc.*, 2010, **132**, 17678–17679.

22 S. Jin, S. Wang, Y. Song, M. Zhou, J. Zhong, J. Zhang, A. Xia, Y. Pei, M. Chen, P. Li and M. Zhu, *J. Am. Chem. Soc.*, 2014, **136**, 15559–15565.

23 M. Brust, M. Walker, D. Bethell, D. J. Schiffrin and R. Whyman, *J. Chem. Soc., Chem. Commun.*, 1994, 801–802, DOI: 10.1039/C39940000801.

24 R. L. Donkers, D. Lee and R. W. Murray, *Langmuir*, 2004, **20**, 1945–1952.

25 T. U. B. Rao and T. Pradeep, *Angew. Chem., Int. Ed.*, 2010, **49**, 3925–3929.

26 X. Meng, Q. Xu, S. Wang and M. Zhu, *Nanoscale*, 2012, **4**, 4161–4165.

27 T. U. B. Rao, B. Nataraju and T. Pradeep, *J. Am. Chem. Soc.*, 2010, **132**, 16304–16307.

28 M. Bodiuzzaman, A. Ghosh, K. S. Sugi, A. Nag, E. Khatun, B. Varghese, G. Paramasivam, S. Antharjanam, G. Natarajan and T. Pradeep, *Angew. Chem., Int. Ed.*, 2019, **58**, 189–194.

29 C. Zeng, Y. Chen, A. Das and R. Jin, *J. Phys. Chem. Lett.*, 2015, **6**, 2976–2986.

30 K. R. Krishnadas, A. Ghosh, A. Baksi, I. Chakraborty, G. Natarajan and T. Pradeep, *J. Am. Chem. Soc.*, 2016, **138**, 140–148.

31 S. Bhat, A. Baksi, S. K. Mudedla, G. Natarajan, V. Subramanian and T. Pradeep, *J. Phys. Chem. Lett.*, 2017, **8**, 2787–2793.

32 R. Gui, H. Jin, Z. Wang and L. Tan, *Coord. Chem. Rev.*, 2015, **296**, 91–124.

33 X. Kang and M. Zhu, *Chem. Soc. Rev.*, 2019, **48**, 2422–2457.

34 M. S. Bootharaju, R. Dey, L. E. Gevers, M. N. Hedhili, J.-M. Basset and O. M. Bakr, *J. Am. Chem. Soc.*, 2016, **138**, 13770–13773.

35 A. Ghosh, M. Bodiuzzaman, A. Nag, M. Jash, A. Baksi and T. Pradeep, *ACS Nano*, 2017, **11**, 11145–11151.

36 C. P. Joshi, M. S. Bootharaju, M. J. Alhilaly and O. M. Bakr, *J. Am. Chem. Soc.*, 2015, **137**, 11578–11581.

37 L. G. AbdulHalim, M. S. Bootharaju, Q. Tang, S. Del Gobbo, R. G. AbdulHalim, M. Eddaoudi, D.-e. Jiang and O. M. Bakr, *J. Am. Chem. Soc.*, 2015, **137**, 11970–11975.

38 B. Li, R.-W. Huang, J.-H. Qin, S.-Q. Zang, G.-G. Gao, H.-W. Hou and T. C. W. Mak, *Chem. – Eur. J.*, 2014, **20**, 12416–12420.

39 X.-J. Xi, J.-S. Yang, J.-Y. Wang, X.-Y. Dong and S.-Q. Zang, *Nanoscale*, 2018, **10**, 21013–21018.

40 P. Chakraborty, A. Baksi, E. Khatun, A. Nag, A. Ghosh and T. Pradeep, *J. Phys. Chem. C*, 2017, **121**, 10971–10981.

41 C. A. Fields-Zinna, J. S. Sampson, M. C. Crowe, J. B. Tracy, J. F. Parker, A. M. de Ney, D. C. Muddiman and R. W. Murray, *J. Am. Chem. Soc.*, 2009, **131**, 13844–13851.

42 G. Kataby, M. Cojocaru, R. Prozorov and A. Gedanken, *Langmuir*, 1999, **15**, 1703–1708.

43 M. van der Linden, A. Barendregt, A. J. van Bunningen, P. T. K. Chin, D. Thies-Weesie, F. M. F. de Groot and A. Meijerink, *Nanoscale*, 2016, **8**, 19901–19909.

44 D. M. Black, N. Bhattarai, R. L. Whetten and S. B. H. Bach, *J. Phys. Chem. A*, 2014, **118**, 10679–10687.

45 M. Farrag, M. Tschurl, A. Dass and U. Heiz, *Phys. Chem. Chem. Phys.*, 2013, **15**, 12539–12542.

46 R.-W. Huang, Y.-S. Wei, X.-Y. Dong, X.-H. Wu, C.-X. Du, S.-Q. Zang and T. C. W. Mak, *Nat. Chem.*, 2017, **9**, 689–697.